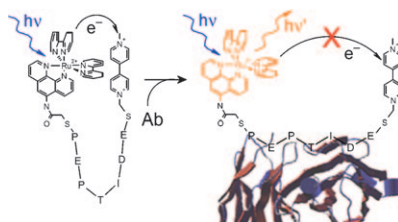


CONCEPTS

Biosensors

K. J. Oh, K. J. Cash,
K. W. Plaxco* 2244–2251

Beyond Molecular Beacons: Optical Sensors Based on the Binding-Induced Folding of Proteins and Polypeptides



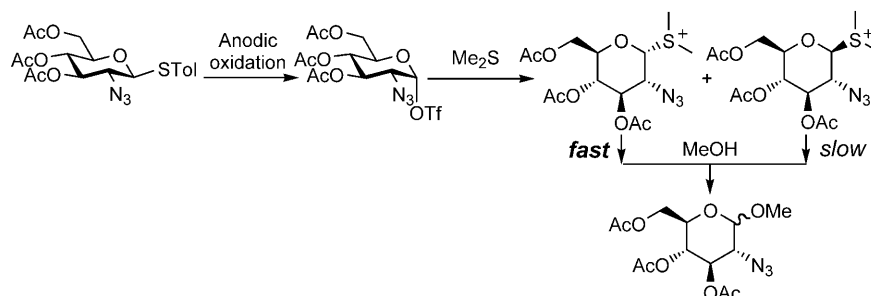
A beacon in the night! The binding-induced folding of otherwise unfolded biopolymers may prove a generic signal-transduction mechanism for protein- and polypeptide-based biosensors. An example of such a biosensor is illustrated here.

COMMUNICATIONS

Carbohydrates

T. Nokami, A. Shibuya, S. Manabe,*
Y. Ito, J. Yoshida* 2252–2255

α - and β -Glycosyl Sulfonium Ions: Generation and Reactivity



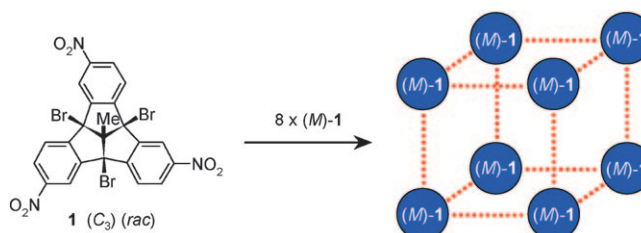
Low-temperature electrochemical oxidation of thioglycosides gave glycosyl triflates from which glycosyl sulfonium ions were produced (see scheme). The latter were characterized by NMR spectroscopy and cold-spray mass spectrometry as a mixture of α - and β -iso-

mers (45:55). The α -glycosyl sulfonium ion exhibited higher reactivity than the β -glycosyl sulfonium ion in the reaction with methanol, which gave a mixture of α - and β -methyl glycosides (41:59).

Supramolecular Aggregation

J. Strübe, B. Neumann,
H.-G. Stammler,
D. Kuck* 2256–2260

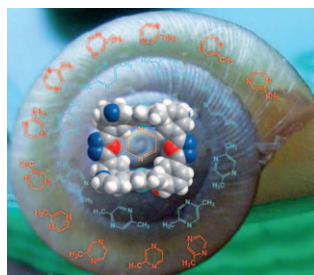
Solid-State Enantiopure Organic Nanocubes Formed by Self Organization of a C_3 -Symmetrical Tribenzotriquinacene



Cubic aggregation: The racemic C_3 -symmetrical tribenzotriquinacene **1** was synthesized and found to crystallize in cubic aggregates consisting of eight homochiral molecules. The major driving force for this unique supramolecular aggregation may be attributed

to the 24 equivalent sub-van der Waals interactions between the bromine atoms located at the convex surface of the triquinacene cores, rather than to polar interactions between the nitrobenzene units within and between the nanocubes.

Squashy cage: A flexible, spongelike, and reversible metal-binding Cu_2L_2 cage that can adjust its internal space in response to pyrazine and its derivatives based on a recognition sequence of pyrazine, 2,5-dimethylpyrazine, and 2-methylpyrazine (see figure) is described.



Reversible Encapsulation

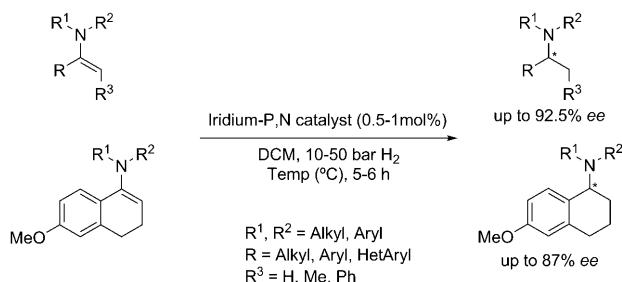
G.-G. Hou, J.-P. Ma, T. Sun,
Y.-B. Dong,*
R.-Q. Huang 2261–2265

A Binuclear Cu^{II} Metallacycle Capable of Discerning between Pyrazine and Its Different Methyl-Substituted Derivatives Based on Reversible Intracage Metal–Ligand Binding

Asymmetric Catalysis

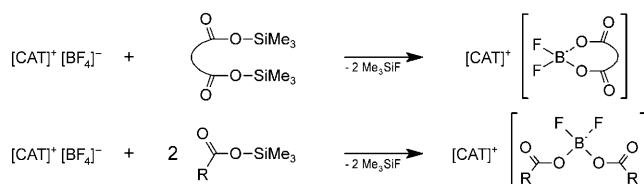
A. Baeza, A. Pfaltz* 2266–2269

Iridium-Catalyzed Asymmetric Hydrogenation of Unfunctionalized Enamines



Optically active tertiary amines are readily prepared by iridium-catalyzed asymmetric hydrogenation of unfunctionalized enamines (see scheme). The best enantioselectivities with > 90 % *ee* were obtained with *N*-aryl- and *N*-

benzyl-substituted enamines with a terminal double bond. The hydrogenation of enamines derived from cyclic ketones, which has not been reported yet with other catalysts, gave enantiomeric excesses of up to 87 %.



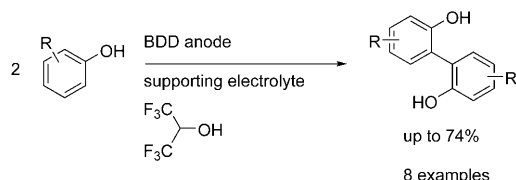
Chloride avoided! A new chloride-free method to synthesise ionic liquids (ILs) with mixed borate anions, starting from tetrafluoroborate compounds, has been developed and a number of examples including some new ILs are

presented (see scheme; $[\text{CAT}]^+ =$ cation). It is widely applicable and allows access to mixed borates with various types of ligands in a straightforward manner.

Ionic Liquids

C. Schreiner, M. Amereller,
H. J. Gores* 2270–2272

Chloride-Free Method to Synthesise New Ionic Liquids with Mixed Borate Anions



Enlarged scope by fluorinated mediators: Oxyl radicals are easily formed on boron-doped diamond (BDD) electrodes and can be exploited for the *ortho*-selective coupling to the corre-

sponding biphenols (see scheme). At partial conversion, a clean transformation is achieved that can be applied to electron-rich as well as fluorinated phenols.

Electroorganic Synthesis


A. Kirste, M. Nieger, I. M. Malkowsky,
F. Stecker, A. Fischer,
S. R. Waldvogel* 2273–2277

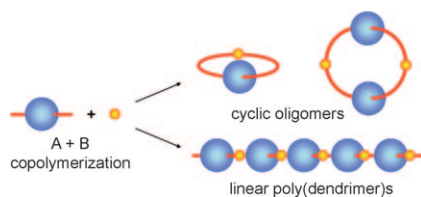
***ortho*-Selective Phenol-Coupling Reaction by Anodic Treatment on Boron-Doped Diamond Electrode Using Fluorinated Alcohols**

FULL PAPERS

Dendrimers

S.-Y. Cheung, H.-F. Chow,* T. Ngai,
X. Wei 2278–2288


 **Synthesis of Organometallic Poly(dendrimer)s by Macromonomer Polymerization: Effect of Dendrimer Size and Structural Rigidity on the Polymerization Efficiency**

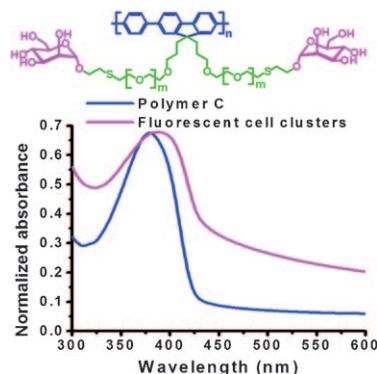


Cyclization versus propagation: The copolymerization behavior of a dendritic macromonomer with a metal-containing linker is controlled by the dendrimer size and its structural rigidity. Structurally more flexible dendritic monomers tend to form more cyclic oligomers than structurally rigid monomers (see figure).

Conjugated Glycopolymers

C. Xue, S. Velayudham, S. Johnson,
R. Saha, A. Smith, W. Brewer,
P. Murthy, S. T. Bagley,
H. Liu* 2289–2295


 **Highly Water-Soluble, Fluorescent, Conjugated Fluorene-Based Glycopolymers with Poly(ethylene glycol)-Tethered Spacers for Sensitive Detection of *Escherichia coli***

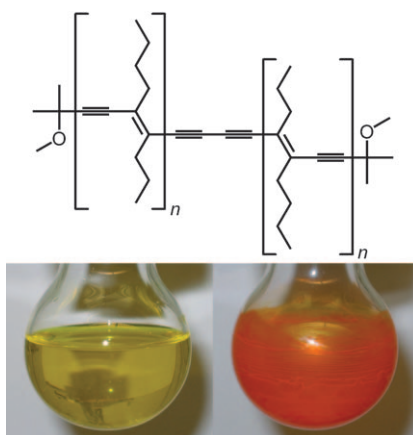


Know your bacteria! Two fluorene-based, conjugated polymers with oligo(ethylene glycol)- and poly(ethylene glycol)-tethered spacers have been prepared by the Suzuki coupling polymerization reactions. β -Glucose and α -mannose residues were covalently attached to the conjugated polymers by post-polymerization functionalization with thiol-functionalized carbohydrates under basic conditions. Investigations on their use as biosensing materials for the detection of *Escherichia coli* are reported (see figure).

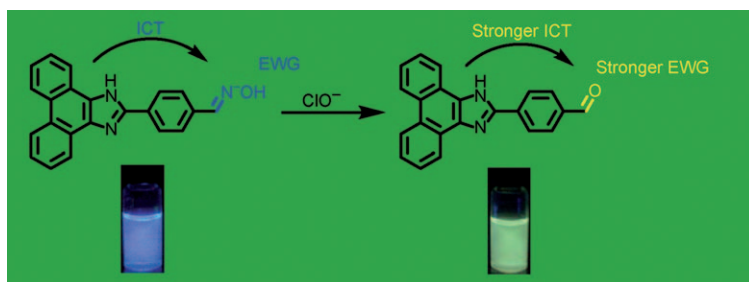
Oligodiacetylenes

G. S. Pilzak, J. Baggerman,
B. van Lagen, M. A. Posthumus,
E. J. R. Sudhölter,
H. Zuilhof* 2296–2304

 **Synthesis and Optoelectronic Properties of Nanometer-Sized and Highly Soluble Homocoupled Oligodiacetylenes**



Color and shape of oligodiacetylenes: We synthesized a series of highly soluble homocoupled oligodiacetylenes (HODAs). The color of these oligomers is dependent on the molecular length and aggregation state (see picture). The optical properties of these materials were studied by using both steady-state and time-resolved spectroscopic techniques.



The first ratiometric fluorescent probe for hypochlorite has been developed through regulation of the electron-withdrawing ability of the electron

acceptor in an intramolecular charge-transfer (ICT) system by a deoximation reaction (see figure; EWG = electron-withdrawing group).

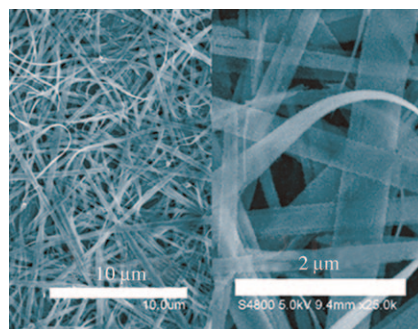
Fluorescent Probes

W. Lin,* L. Long, B. Chen,
W. Tan 2305–2309

A Ratiometric Fluorescent Probe for Hypochlorite Based on a Deoximation Reaction



Molecular highways: A facile one-step, surfactant-free route was applied to produce high-purity and uniform α - MoO_3 nanoribbons (see figure), and their photocatalytic, photoconductive, and electrochemical properties were investigated. The results showed that the as-prepared products had superior photo and electro properties.



Molybdenum Nanoribbons

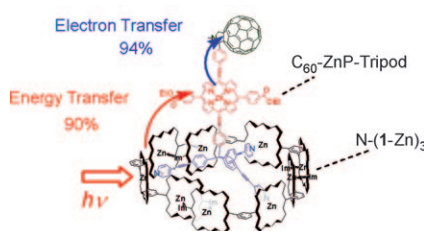
L. Cheng, M. Shao,* X. Wang,
H. Hu 2310–2316

Single-Crystalline Molybdenum Trioxide Nanoribbons: Photocatalytic, Photoconductive, and Electrochemical Properties



A mimic for nature's solar cells:

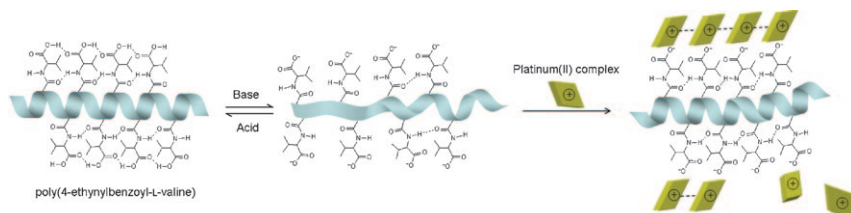
Simple mixing of nonaporphyrin macrocycle N-(1-Zn)₃ and acceptor ligand C₆₀-ZnP-Tripod affords a supramolecular architecture (see scheme), in which the excitation energy collected by the macrocycle is transferred efficiently to the central ZnP acceptor, inducing charge separation between the ZnP and C₆₀ sites.



Photochemistry

Y. Kuramochi, A. S. D. Sandanayaka,
A. Satake, Y. Araki, K. Ogawa, O. Ito,*
Y. Kobuke* 2317–2327

Energy Transfer Followed by Electron Transfer in a Porphyrin Macrocycle and Central Acceptor Ligand: A Model for a Photosynthetic Composite of the Light-Harvesting Complex and Reaction Center



The aggregation and self-assembly of square-planar alkynylplatinum(II) complexes is induced by the use of a chiral polyacetylene with a helical conformation (see scheme). The chain

helicity of the chiral polyacetylene under basic conditions has also been demonstrated to be enhanced by the presence of the positively charged platinum(II) complexes.

Transition-Metal Photophysics

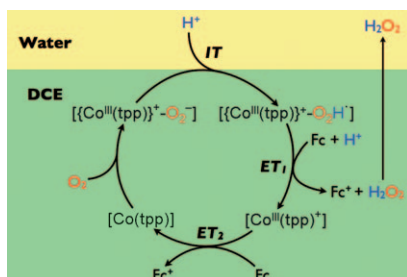
K. H.-Y. Chan, J. W.-Y. Lam,
K. M.-C. Wong, B.-Z. Tang,*
V. W.-W. Yam* 2328–2334

Chiral Poly(4-ethynylbenzoyl-L-valine)-Induced Helical Self-Assembly of Alkynylplatinum(II) Terpyridyl Complexes with Tunable Electronic Absorption, Emission, and Circular Dichroism Changes

Catalysis

R. Partovi-Nia, B. Su, F. Li, C. P. Gros,
J.-M. Barbe, Z. Samec,
H. H. Girault* 2335–2340

Proton Pump for O₂ Reduction Catalyzed by 5,10,15,20-Tetraphenylporphyrinatocobalt(II)



Oxygen reduction: A polarized water|1,2-dichloroethane (DCE) interface acts as a proton pump for the [Co(tpp)] (TPP = 5,10,15,20-tetraphenylporphyrinato) catalyzed O₂ reduction by ferrocene (Fc) compounds to produce H₂O₂ (see figure; IT = ion transfer, ET = electron transfer). This system favours the collection of H₂O₂ by extraction immediately after its formation in DCE to the adjacent water phase.

Heterogeneous Catalysis

K.-i. Shimizu,* K. Sugino, K. Sawabe,
A. Satsuma 2341–2351

Oxidant-Free Dehydrogenation of Alcohols Heterogeneously Catalyzed by Cooperation of Silver Clusters and Acid–Base Sites on Alumina

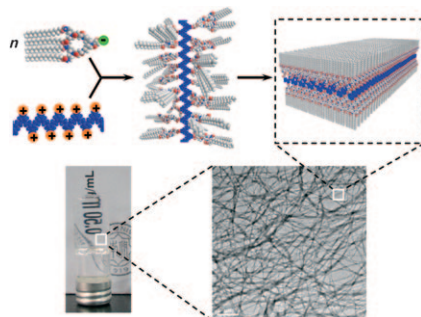


Trifunctional green catalysis: In-depth characterization shows that oxidant-free selective oxidation of alcohols by silver nanoparticles on γ -Al₂O₃, as a new heterogeneous catalyst, proceeds through cooperation of silver, acid, and base sites (see figure).

Gelation

Z. Zhang, M. Yang, X. Zhang,
L. Zhang, B. Liu, P. Zheng,
W. Wang* 2352–2361

Enhancing Gelation Ability of a Dendritic Gelator through Complexation with a Polyelectrolyte

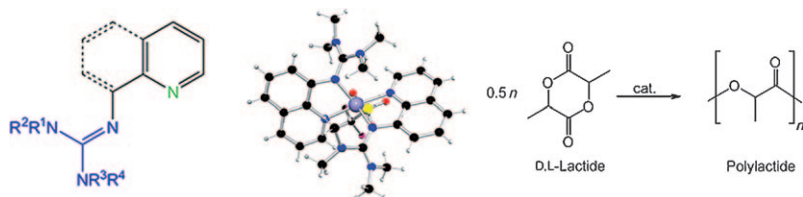


Let's stick together: The gelation ability of a dendritic gelator has been enhanced by its complexation with a polyelectrolyte (see figure). This concept provides a route to construct novel functional or ordered materials by complexation of other low-molecular-mass functional species with polyelectrolytes.

Sustainable Chemistry

J. Börner, U. Flörke, K. Huber,
A. Döring, D. Kuckling,
S. Herres-Pawlis* 2362–2376

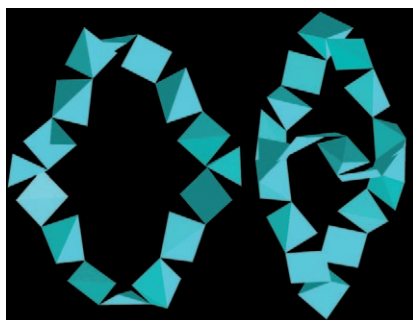
Lactide Polymerisation with Air-Stable and Highly Active Zinc Complexes with Guanidine–Pyridine Hybrid Ligands



New class of air-stable catalysts for lactide polymerisation: Guanidine–pyridine hybrid ligands (picture, left) were used to prepare a series of zinc complexes (e.g., depicted cation [ZnL₂-(CF₃SO₃)⁺], where L is the quinoline-containing ligand with R¹ = R² = R³ =

R⁴ = Me), in which the ligand binds through two different N-donor atoms. The zinc complexes show high activity in ring-opening polymerisation of D,L-lactide (right), giving polylactide with molecular masses up to 176 000 g mol^{−1} and in high yield.

Copper clusters: Two high-nuclearity copper cages, tricornic Cu_{21} and saddle-like cyclic Cu_{16} (see pictures), were synthesized. Magnetic studies and Monte Carlo calculations were also performed to show the overall anti-ferromagnetic properties of the two compounds.



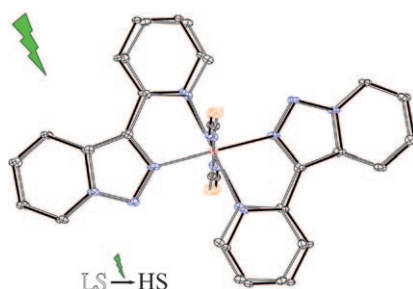
Metallocages

Y.-L. Bai, V. Tangoulis,* R.-B. Huang, L.-S. Zheng, J. Tao* 2377–2383

Self-Assembly of High-Nuclearity Copper Cages: Tricornic Cu_{21} and Saddlelike Cyclic Cu_{16}



Switchable molecules: The electronic configurations of the Fe center in *trans*- $[\text{Fe}(\text{tzpy})_2(\text{NCS})_2]$ in low-spin, high-spin, and LIESST states (LIESST = light-induced excited spin-state trapping) were confirmed by K- and L-edge X-ray absorption and magnetic measurements. The molecular structures at 40 K before and after irradiation are superimposed in the picture, which demonstrates a single-crystal-to-single-crystal transition by irradiation.

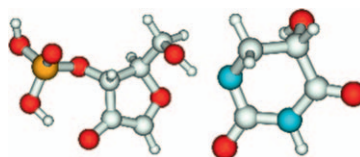


Spin-State Trapping

C.-F. Sheu, K. Chen, S.-M. Chen, Y.-S. Wen, G.-H. Lee, J.-M. Chen, J.-F. Lee, B.-M. Cheng, H.-S. Sheu, N. Yasuda, Y. Ozawa, K. Toriumi, Y. Wang* 2384–2393

Structure and Electronic Configuration of an Iron(II) Complex in a LIESST State: A Pump and Probe Method

Cutting ties: Strand scission and base release in hydroxy-radical adducts of 3'-uridine monophosphate (UMP) have been explored by using density functional theory. The presence of the ribose 2'-OH group and the resultant formation of low-barrier hydrogen bonds with oxygen atoms of the 3'-phosphate linkage are highly important for hydrogen transfer and the subsequent bond-breakage reactions (see picture).



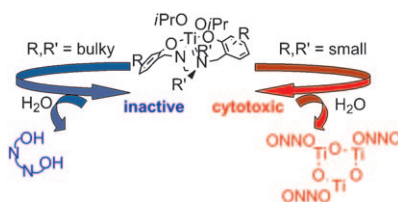
RNA Strand Scission

R. b. Zhang, L. A. Eriksson* 2394–2402

Distinct Hydroxy-Radical-Induced Damage of 3'-Uridine Monophosphate in RNA: A Theoretical Study



Carefully design your ligand! A new family of highly cytotoxic Ti^{IV} complexes demonstrates strong dependence of activity on the particular ligand employed, in which small structural modifications dramatically affect both hydrolytic behavior and biological activity (see picture). Different structure-dependence patterns are observed for hydrolysis and cytotoxicity, which are, nonetheless, strongly related.



Ti^{IV} Complexes

D. Peri, S. Meker, M. Shavit, E. Y. Tshuva* 2403–2415

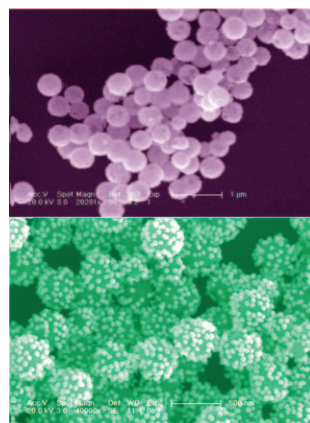
Synthesis, Characterization, Cytotoxicity, and Hydrolytic Behavior of C_2 - and C_1 -Symmetrical Ti^{IV} Complexes of Tetradentate Diamine Bis(Phenolato) Ligands: A New Class of Antitumor Agents



Nanostructures

S. Guo, S. Dong, E. Wang* 2416–2424

A General Route to Construct Diverse Multifunctional Fe₃O₄/Metal Hybrid Nanostructures

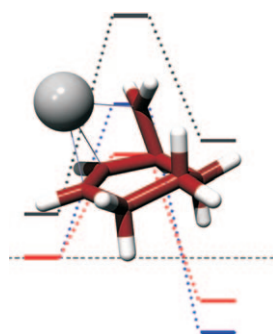


Multifunctional nanostructures: By using 3-aminopropyltrimethoxysilane as a linker, Au nanoparticles (NPs), Au shells, flowerlike Au/Pt hybrid NPs, and Ag or Au/Ag core/shell NPs could be supported on the surface of superparamagnetic Fe₃O₄ spheres to construct hybrid nanostructures that display near-IR absorption, high catalytic activity towards an electron-transfer reaction, or excellent surface-enhanced Raman scattering activity. The picture shows SEM images of Fe₃O₄ spheres coated with Au shells (top) and with Au/Pt hybrid NPs (bottom).

Radicals

C. M. Jäger, M. Hennemann,
T. Clark* 2425–2433

The Effect of a Complexed Lithium Cation on a Norcarane-Based Radical Clock

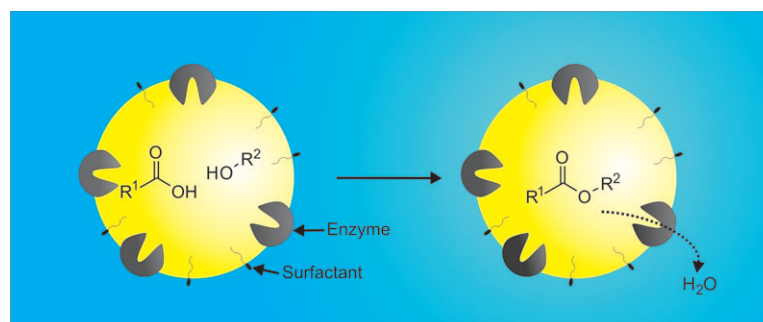


Making radical clocks run faster: Complexation of the 2-norcaranyl radical to the “naked” lithium cation lowers the barrier to the “radical-clock” rearrangement (see picture). However, model calculations on the mechanism of the hydroxylation of norcarane with cytochrome P450 suggest that no such electrostatic catalysis can be expected at the active site of the enzyme.

Enzyme Catalysis

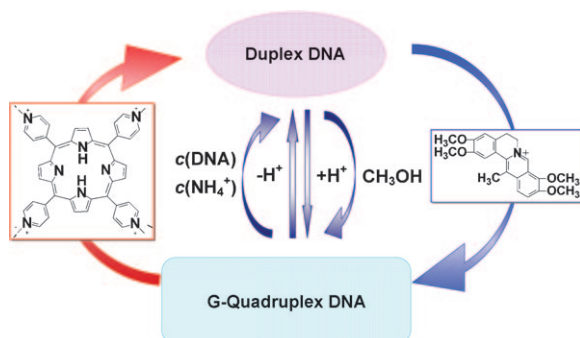
E. M. Aschenbrenner, C. K. Weiss,*
K. Landfester 2434–2444

Enzymatic Esterification in Aqueous Miniemulsions



Just a drop of water: Esterification in water is possible by confining the reactants in small miniemulsion droplets protected by nonionic surfactants. A lipase located at the interface between the droplet and aqueous surroundings

catalyzes the esterification and expels generated water from the reaction site (see picture). High yields of the ester can be obtained after short reaction times under ambient conditions.



Which form to take? The interconversion between the G-quadruplex and duplex DNA forms in the *bcl-2* promoter could be induced by fluctuations in the pH value or DNA and NH_4^+

concentrations, by adding CH_3OH , and by introducing small molecules (cationic porphyrin and dehydrocorydoline; see scheme).

DNA Structures

H. H. Li, Y. Q. Liu, S. Lin,
G. Yuan* 2445–2452

Spectroscopy Probing of the Formation, Recognition, and Conversion of a G-Quadruplex in the Promoter Region of the *bcl-2* Oncogene



* Author to whom correspondence should be addressed



Supporting information on the WWW (see article for access details).



Full Papers labeled with this symbol have been judged by two referees as being "very important papers".



A video clip is available as Supporting Information on the WWW (see article for access details).

SERVICE

Spotlights 2240 Author Index 2454 Keyword Index 2455 Preview 2459

Issue 9/2009 was published online on February 6, 2009

